Ab Initio Calculations of the Structures and Vibrational Spectra of Ethene Complexes

Bruce D. Alexander*,† and Trevor J. Dines*

Division of Physical and Inorganic Chemistry, Carnelley Building, University of Dundee, Dundee, DD1 4HN, U.K.

Received: June 16, 2003; In Final Form: October 3, 2003

To facilitate an objective comparison of the efficacy of the simulation of structural parameters and vibrational spectra of transition-metal complexes of commonly used ab initio methods, the geometries of the ethene complexes of Ni(0) and Ni(II) have been optimized using both ab initio and density functional theory (DFT) calculations and a wide variety of basis sets. The harmonic vibrational spectra of $[Ni(C_2H_4)]$ and $[Ni(C_2H_4)]^{2+}$ have been evaluated from the optimized geometries at Hartree−Fock, post-Hartree−Fock Møller−Plesset perturbation theory, MP2, and a range of DFT functionals. Upon comparison with experimental data, it has been found that hybrid DFT functionals, specifically B3-LYP, afford the most accurate fit to the experimental data. This is especially the case when using the all-electron DZVP basis set, which provides highly accurate results. The use of the effective core potential LanL2DZ basis set has been found to achieve a comparable level of accuracy to the DZVP basis set, at a fraction of the computational efficiency. Extension of these calculations to ethene complexes of other transition metals has revealed trends in their structures and vibrational spectra.

Introduction

Transition-metal complexes of unsaturated hydrocarbons, such as ethene and ethyne, are of significant interest due to their importance in both homogeneous and heterogeneous catalysis. For example, the cyclo-oligomerization, hydrogenation, polymerization, and metathesis reactions of alkenes and alkynes are known to be catalyzed by Ni(0) complexes.[1−6] The importance of nickel complexes and surfaces has led to many reports on the preparation of model complexes considered to be relevant to catalysis and many theoretical studies of the nature of the bonding.[7−18] The precise nature of the bonding between transition metals and unsaturated hydrocarbons continues to be a subject of a great deal of interest owing to the increasing accessibility of more sophisticated model complexes, coupled with increasing computational capabilities.

Most studies concur that the bonding between nickel and an unsaturated hydrocarbon generally follows the Dewar−Chatt−Duncanson (DCD) model.[19,20] The basis of the DCD model is that a σ bond is formed between a metal $(n-1)$d ns np^2 hybrid orbital and the π orbital of ethene. A π bond is also formed between the metal $(n-1)$d orbital and the hydrocarbon π^* orbital. Chatt and Duncanson proposed that the π bond would be stabilized by the hybridization of the filled $(n-1)$d orbital with a vacant np orbital. The dp hybrid orbital would increase the overlap between metal and hydrocarbon orbitals compared with the overlap between the metal nd and the hydrocarbon π^* orbital.

Given the level of interest in the transition-metal−olefin complexes along with the somewhat broad nature of the theoretical model chemistries employed, it is therefore of importance to evaluate the relative merits of different levels of theory and basis sets commonly found in current use for similar model systems. This paper reports such a systematic study into the efficiency and accuracy of a variety of model chemistries, which are commonly used for modeling geometric structure and vibrational spectra. This study has been applied to small transition-metal−hydrocarbon systems with the aim of highlighting the most effective computational approach for modeling much larger inorganic complexes, and their relevance to species adsorbed on metal surfaces is also discussed.

Computational Details

All calculations were performed using the Gaussian 98 program,[21] initially at the Hartree−Fock and B3-LYP levels using a variety of Pople-type split-valence basis sets, along with the DZVP, DZVP2, and LanL2DZ basis sets.[22−24] Unlike the Pople basis sets, the DZVP and DZVP2 basis sets have been optimized specifically for use with DFT methods. The DZVP basis set is a double-ζ quality split-valence basis set with p-type polarization functions added to first row transition metals, d- and p-type functions added to first-row atoms,[25,26] and s-type functions added to the hydrogen atoms and is similar to Pople's 6-31G(d) basis set.[27] The DZVP2 basis set is similar to the DZVP basis set but has d-type polarization functions added to first-row transition metals and p-type polarization functions added to the hydrogen atoms. The LanL2DZ basis set is an effective core potential (ECP) basis set which utilizes the Dunning−Huzinaga double-ζ (DZ) basis functions[28] for carbon and hydrogen atoms along with the Los Alamos effective core potential for the Ni core electrons with DZ functions for Ni valence orbitals.[22−24]

Geometry optimizations and harmonic wavenumber calculations for the singlet ground state of $[Ni(C_2H_4)]$ were performed using the LanL2DZ or DZVP basis sets along with a wide range of density functionals. These include "pure" DFT methods such as SVWN, PW91-LYP, G96-LYP, BLYP, and MPW-PW91,

* Authors to whom correspondence should be addressed. E-mail: t.j.dines@dundee.ac.uk (T.J.D.); bruce.alexander@chiam.unige.ch (B.D.A.). Fax: 44-1382-345517 (T.J.D.).

† Present address: Applied Chemistry, University of Geneva, Sciences II, 30 quai E.-Ansermet, 1211 Geneva, CH. E-mail: bruce.alexander@chiam.unige.ch.

10.1021/jp0357020 CCC: $27.50
Published on Web 12/04/2003

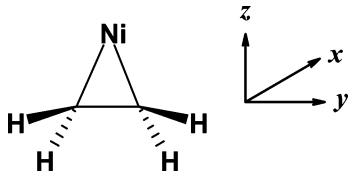

Figure 1. Definition of axes for [Ni(C_2H_4)].

where G96 denotes Gill's exchange 1996 functional,[29,30] MPW denotes the 1991 exchange functional of Perdew and Wang as modified by Barone,[31] LYP signifies the Lee−Yang−Parr correlation functional,[32] and PW91 denotes the Perdew−Wang 1991 gradient corrected exchange and correlation functionals.[33−35] The MPW1-PW91, B3-PW91, B3-P86, BH and H, BH and HLYP, B1-LYP, and B3-LYP "hybrid" DFT methods were also used. Here B1 and B3 signify Becke's one- and three-parameter exchange functionals,[36,37] respectively, MPW1 denotes the one-parameter-modified Perdew−Wang exchange functional,[31] and P86 denotes Perdew's 1986 correlation functional.[38] The BH and H method treats the exchange energy as a "half-and-half" mix of Hartree−Fock and LSDA functionals with the LYP correlation functional; BH and H contains an additional contribution from Becke's 1988 exchange functional. These methods are implemented in Gaussian 98 in a manner similar to, although not the same as, that suggested by Becke.[39]

In all cases, the [Ni(C_2H_4)] geometry was initially optimized in the C_{2v} point group, which was then modified accordingly, by eigenvector following, when large imaginary wavenumbers were obtained. The definition of the coordinate system used in conjunction with the C_{2v} point group is shown in Figure 1, where the *yz* plane contains the heavier atoms. Thus the 15 vibrational modes transform as $\Gamma_{3N-6} = 5a_1 + 3a_2 + 3b_1 + 4b_2$. All of the normal modes are Raman active, whereas only modes of a_1, b_1, and b_2 symmetry are IR active. For computation of IR and Raman spectra and the potential-energy distributions associated with the vibrational modes, the Cartesian force constants dipole derivatives and, when possible, polarizability derivatives obtained from the Gaussian 98 output were expressed in terms of internal coordinates. Scaling factors, where necessary, were applied to the force constants before input to a normal coordinate analysis program derived from those of Schachtschneider.[40] Polarizability derivatives, and therefore Raman intensities, were calculated numerically at the DFT level, where applicable. Normal coordinate analysis was initially performed without scaling. When reported, scaled normal coordinate analysis follows the scaling method of Pulay[41] to obtain the best fit of the calculated wavenumbers to the experimental data.

Results and Discussion

The Effect of Basis Set on the Equilibrium Geometries of [Ni(C_2H_4)] and [Ni(C_2H_4)]$^{2+}$. The optimized geometries of [Ni(C_2H_4)] calculated at the B3-LYP level using different basis sets are given in Table 1; also included for comparison are experimental data from crystal structures of ethene complexes with nickel[42,43] and structural data taken from single-crystal surface studies.[44,45] The variation in geometric parameters with basis set is also represented diagrammatically, in Figure 2. As the size of the basis set increases, a steady decrease in *r*(CC) can be observed. When compared with the carbon−carbon bond lengths determined for ethene adsorbed on a Ni(111) surface,[44] the ECP LanL2DZ basis set affords the closest fit whereas the DZVP basis set better reproduces *r*(CC) found in nickel−ethene complexes.[42,43] Bond angles are at best within 2° of experimental values. The θ(oop) parameter is defined as the angle by which the hydrogens lie out of the plane of an unperturbed ethene molecule. Thus, it is a measure of the restructuring, or distortion, of the ethene moiety induced by the metal center and is therefore a valuable indication of the bonding between the nickel atom and the ethene moiety. B3-LYP calculations consistently predict small θ(oop) values, thus inferring only slight restructuring. Increasing the size of the basis set shows a decrease in θ(oop). The most accurate bond angles are provided by the DZ-type basis sets.

TABLE 1: Geometric Parameters[a] of [Ni(C_2H_4)] Calculated at the B3-LYP Level

basis set	*r*(CH)	*r*(CC)	*r*(NiC)	θ(NiCC)	θ(CNiC)	θ(oop)	θ(HCH)
3-21G	1.089	1.501	1.757	64.7	50.6	20.9	112.1
6-31G	1.092	1.470	1.827	66.3	47.4	19.1	111.8
6-31G(d)	1.094	1.461	1.817	66.3	47.4	18.9	111.7
6-31G(d,p)	1.094	1.461	1.816	66.3	47.4	19.0	111.7
6-311G	1.089	1.452	1.864	67.1	45.9	17.5	112.9
6-311G(d)	1.092	1.442	1.860	67.2	45.6	17.1	112.9
6-311G(d,p)	1.090	1.442	1.858	67.2	45.7	16.8	113.1
LanL2DZ	1.093	1.450	1.918	67.8	44.4	14.3	114.4
DZVP	1.093	1.434	1.892	67.7	44.5	14.2	114.2
DZVP2	1.092	1.439	1.885	67.6	44.9	14.6	114.2
exp[b]		1.431	1.991	69.8	42.1		
exp[c]		1.400	1.978	69.3	41.4		
exp[d]		1.450					
exp[e]		1.390					117.0

[a] Bond lengths in Å, bond angles in degrees. [b] [Ni(C_2H_4)(PPh_3)$_2$], ref 43. [c] [(tmeda)Ni(C_2H_4)(H_2CO)], tmeda = tetramethylethylenediamine, ref 42. [d] C_2H_4 adsorbed on Ni(111), ref 44. [e] C_2H_4 adsorbed on Ni(111), ref 45.

It should be noted that no experimental structure for [Ni(C_2H_4)] has been reported thus far. Consequently, the comparison of the experimental geometries given in Table 1 with the results of the ab initio calculations is not strictly a comparison of "like with like". Nevertheless, comparison of the optimized geometries of [Ni(C_2H_4)] with the crystal structures of nickel(0) complexes offers good indication as to the accuracy of the computational method. Table 1 shows that the ethene bond lengths and angles are satisfactorily reproduced at the B3-LYP level. This is especially the case for the DZVP and DZVP2 basis sets and, to a lesser extent, the LanL2DZ basis set. However, *r*(NiC) is poorly reproduced throughout the variety of basis sets employed, and the LanL2DZ basis set affords the best fit to experimental data although this remains 0.07 Å too short. The disparity between experimental carbon−nickel bond lengths and those calculated at the B3-LYP level is likely to be due to the presence of electron-donating triphenylposphine ligands[43] or tetramethylethylenediamine ligands.[42] It is interesting to note that B3-LYP/LanL2DZ level calculations on [Ni(PH_3)$_2$(C_2H_4)] and [Ni(PH_3)$_2$(C_2H_4)$_2$] have yielded *r*(NiC) values of 1.986 and 2.087 Å, respectively.[46] This has also been found to be the case at the B3-LYP/DZVP level;[47] thus the presence and nature of additional ligands, such as phosphine groups, elongates the carbon−nickel bond. This is reflected in both experimental data and in the ab initio calculations.

It is of further interest to compare the B3-LYP/DZVP and B3-LYP/DZVP2 calculations for [Ni(C_2H_4)] with those of Bernardi et al., who reported optimized geometries for isomers of [Ni(C_2H_4)] for a variety of DFT methods using the DZVP basis set.[18] For each isomer, Bernardi et al. predicted carbon−nickel bond lengths that were consistently 0.1 Å larger than those reported in Table 1. Unsurprisingly, the environment of the central nickel atom is crucial when trying to attain accurate carbon−nickel bond distances. This is further evidenced by models of ethene adsorption on a Ni(100) surface using a nine-atom nickel cluster.[48] The ethene−surface distance was found

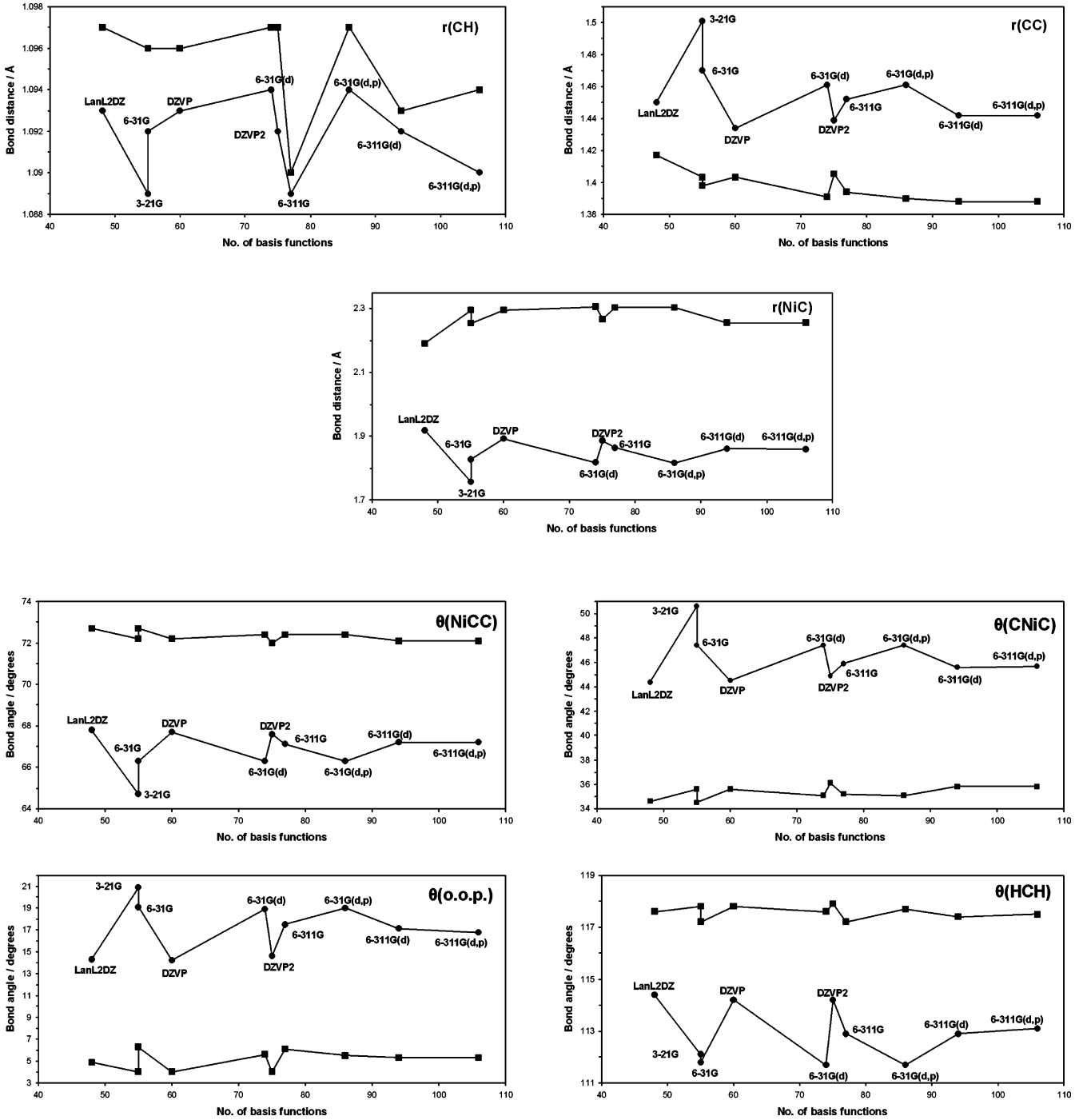

Figure 2. The effect of basis set on the geometric parameters of $[Ni(C_2H_4)]$ (● = labeled) and $[Ni(C_2H_4)]^{2+}$ (■ = unlabeled), calculated at the B3-LYP level.

to be 1.869 Å for di-σ bonded and 1.908 Å for $\pi-$bonded ethene at the B3-LYP/LanL2DZ level using a "frozen" nickel cluster where the nickel−nickel bonds were fixed. This compares with the present value of 1.892 Å from Table 1. When modeling metal surfaces, the inclusion of many surface atoms is of undoubted importance. Given that the comparison of the present geometric parameters with literature values indicates the importance of the local environment of the metal surface atom, it seems likely that, to model adsorption properly, optimization of the metal cluster *must* also be performed. This would be the case especially when considering adsorption energies, as inclusion of surface reconstruction or relaxation would be crucial to the success of any model and it is clearly not sufficient to treat an adsorbed species by using only one metal atom.

The calculated geometry of $[Ni(C_2H_4)]^{2+}$ is reported in Table 2, and the variation with size of basis set is also shown in Figure 2. It is clear that r(CC) is much shorter than that for the neutral complex. A more positive charge on the nickel has the effect of increasing r(NiC) by ca. 0.5 Å. Addition of polarization functions to the basis set has a more marked effect for the cationic species than the neutral one. Addition of the first-polarization d functions reduces r(NiC) by 0.04 Å in most cases, except on going from B3-LYP/6-31G to B3-LYP/6-31G(d) where an increase is observed. The bond angles involving the nickel atom reflect the differing behavior of the carbon−carbon bond with charge. For the cationic species, an increase in level of theory causes a decrease in θ(NiCC) and an increase in θ(CNiC), opposite to that calculated for the neutral species. The

TABLE 2: Geometric Parameters[a] of $[Ni(C_2H_4)]^{2+}$ Calculated at the B3-LYP Level

basis set	*r*(CH)	*r*(CC)	*r*(NiC)	*θ*(NiCC)	*θ*(CNiC)	*θ*(oop)	*θ*(HCH)
3-21G	1.096	1.403	2.296	72.2	35.6	4.0	117.8
6-31G	1.096	1.398	2.254	72.7	34.5	6.3	117.2
6-31G(d)	1.097	1.391	2.306	72.4	35.1	5.6	117.6
6-31G(d,p)	1.097	1.390	2.304	72.4	35.1	5.5	117.7
6-311G	1.090	1.394	2.304	72.4	35.2	6.1	117.2
6-311G(d)	1.093	1.388	2.256	72.1	35.8	5.3	117.4
6-311G(d,p)	1.094	1.388	2.256	72.1	35.8	5.3	117.5
LanL2DZ	1.097	1.417	2.192	72.7	34.6	4.9	117.6
DZVP	1.096	1.403	2.296	72.2	35.6	4.0	117.8
DZVP2	1.097	1.405	2.268	72.0	36.1	4.0	117.9

[a] Bond lengths in Å, bond angles in degrees.

predicted values of *θ*(oop) show a dramatic decrease in the cationic species compared with the neutral species, reflecting changes in *r*(CC), *θ*(NiCC), and *θ*(CNiC).

Unfortunately, the marked change in geometric parameters observed upon increasing positive charge on the nickel atom cannot be verified experimentally as no structures have been reported for ethene interacting with a nickel cation. However, it is clear that the ethene moiety is less distorted from its gas-phase structure in $[Ni(C_2H_4)]^{2+}$ than in $[Ni(C_2H_4)]$, directly evidenced by smaller *θ*(oop) angles, which are a sensitive indication of rehybridization of the carbon sp^2 orbitals. In a study of $[XM(C_2H_4)]$, where M is Ag^+ or Cu^+ and X is a halide anion, Huang et al. observed an increased ethylene distortion in the order F > Cl > Br > I, i.e., increased electronegativity of anion increased the ethylene distortion.[49] This was attributed to an increased positive charge on the metal leading to a more favored *π* back donation and thus distortion. That ethene in $[Ni(C_2H_4)]^{2+}$ is less distorted than in $[Ni(C_2H_4)]$ due to the electron deficiency of the cationic species. This results in a decreased donation of electrons from nickel to the *π** antibonding orbital of ethene in the cationic species with respect to the neutral species. Thus, the carbon−carbon bond order lies much closer to 2 in the cationic species and the ethene moiety is less distorted.

Without structural data available for $[Ni(C_2H_4)]^{2+}$ species, it is difficult to comment on the accuracy of the methods used in Table 2. Intuitively, it seems that B3-LYP affords the most realistic geometry, especially when the DZVP basis set is used, and this is best highlighted by comparison of the *r*(NiC) values. It should be noted that Bögel et al. could not obtain structures of $[Ni(C_2H_4)]^{2+}$ at the B3-LYP level,[50] although structures of $[Ni(\eta^4\text{-butadiene})]^{2+}$ were obtained. These structures, which consisted of cis and trans forms of butadiene bound to the nickel ion through all four carbon atoms, were found to be true energy minima.

The Effect of Basis Set on the Vibrational Spectrum of $[Ni(C_2H_4)]$. The effect of basis set on the calculated vibrational spectrum is more complex than the effect on the optimized geometries. Table 3 shows the variation of the unscaled vibrational wavenumbers with basis set at the B3-LYP level for $[Ni(C_2H_4)]$, and this information is shown diagrammatically in Figure 3. No imaginary vibrations are predicted indicating that stable equilibrium geometries are obtained throughout. It should be noted that as the vibrational wavenumbers are unscaled, they are consistently high compared with experimental values. On going from 3-21G to 6-31G to 6-311G basis sets, the *ν*(CH) vibrations decrease in wavenumber. Adding first d- and then p-polarization functions to the 6-31G series has the effect of lowering the *ν*(CH) vibrations. By contrast, addition of polarization functions to the 6-311G series has little effect on *ν*(CH) vibrations. The 6-311G(d,p) basis set best reproduces CH stretching vibrations with the LanL2DZ basis set giving results that are comparable with 3-21G.

The behavior of the hydrogen-bending motions is more complex and this is especially the case for the a_1 vibrations. The a_2, b_1, and b_2 vibrations are usually predicted to occur within a narrow range; i.e., there is little variation in these vibrations with basis set, especially for the a_1 vibrations. However, examination of the potential-energy distribution of the ν_2, ν_3, and ν_4 modes (vide infra) reveals the ν_2 vibration to be associated with $\delta(CH_2)_{sym}$ with varying degrees of mixing with the $\omega(CH_2)_{sym}$ coordinate. In the case of 3-21G, each symmetry coordinate contributes in almost equal amount. The ν_3 mode is predominantly due to $\omega(CH_2)$ with some mixing with the $\delta(CH_2)$ coordinate; although with the 6-311G(d) and 6-311G(d,p) basis sets there is also a small degree of coupling to the *ν*(CC) stretch. The ν_4 mode is attributed to *ν*(CC) with a small degree of coupling to *ν*(NiC) and, in some cases, $\omega(CH_2)$. The ν_3 and ν_4 assignments from LanL2DZ basis set are reversed. The nickel−carbon stretches, ν_5 and ν_{15}, show little variation between the split-valence basis sets. The *ν*(NiC) modes predicted by the LanL2DZ basis set are the lowest and closest to the experimental data, the asymmetric stretch lying 23 cm^{-1} higher than experimental. The DZ-type basis sets tend to predict the lowest ν_5 and ν_{15} modes.

Comparison with experimental data shows that the LanL2DZ, DZVP, and DZVP2 basis sets yield the closest fit to experimental data, even for unscaled vibrations; this is especially evident for the ν_4 and ν_{14} modes. It is particularly satisfying to

TABLE 3: Calculated Vibrational Spectra (cm^{-1}) of $[Ni(C_2H_4)]$ Using the B3-LYP Method

	mode	3-21G	6-31G	6-31G(d)	6-31G(d,p)	6-311G	6-311G(d)	6-311G(d,p)	LanL2DZ	DZVP	DZVP2	exp[a,b]
a_1	ν_1	3101	3091	3073	3065	3056	3057	3057	3102	3087	3095	2965.2
	ν_2	1552	1545	1537	1524	1538	1532	1518	1515	1523	1509	1468.2
	n_3	1119	1121	1123	1119	1142	1151	1149	1169	1175	1167	1165.9
	ν_4	1030	1052	1028	1025	1061	1022	1023	955	931	937	902.0
	ν_5	649	608	617	617	568	570	572	520	528	533	517.4
a_2	ν_6	3145	3141	3119	3116	3111	3109	3112	3176	3159	3163	
	ν_7	1226	1238	1224	1217	1245	1233	1228	1217	1206	1202	
	ν_8	800	822	808	809	871	861	858	819	844	832	
b_1	ν_9	3167	3163	3139	3135	3136	3133	3134	3202	3179	3184	3031.7
	ν_{10}	826	826	802	799	842	820	821	814	797	797	n.o.
	ν_{11}	741	714	700	701	735	719	714	602	632	628	601.8
b_2	ν_{12}	3093	3082	3067	3059	3044	3050	3050	3088	3079	3086	n.o.
	ν_{13}	1509	1504	1481	1467	1496	1474	1460	1462	1447	1441	1386.4
	ν_{14}	1162	1104	1061	1058	1110	1059	1065	988	964	972	907.0[c]
	ν_{15}	685	593	592	591	556	551	552	465	493	495	502.2

[a] From ref 51. [b] n.o. = not obtained. [c] From the $\nu_4 + \nu_{14}$ combination band.

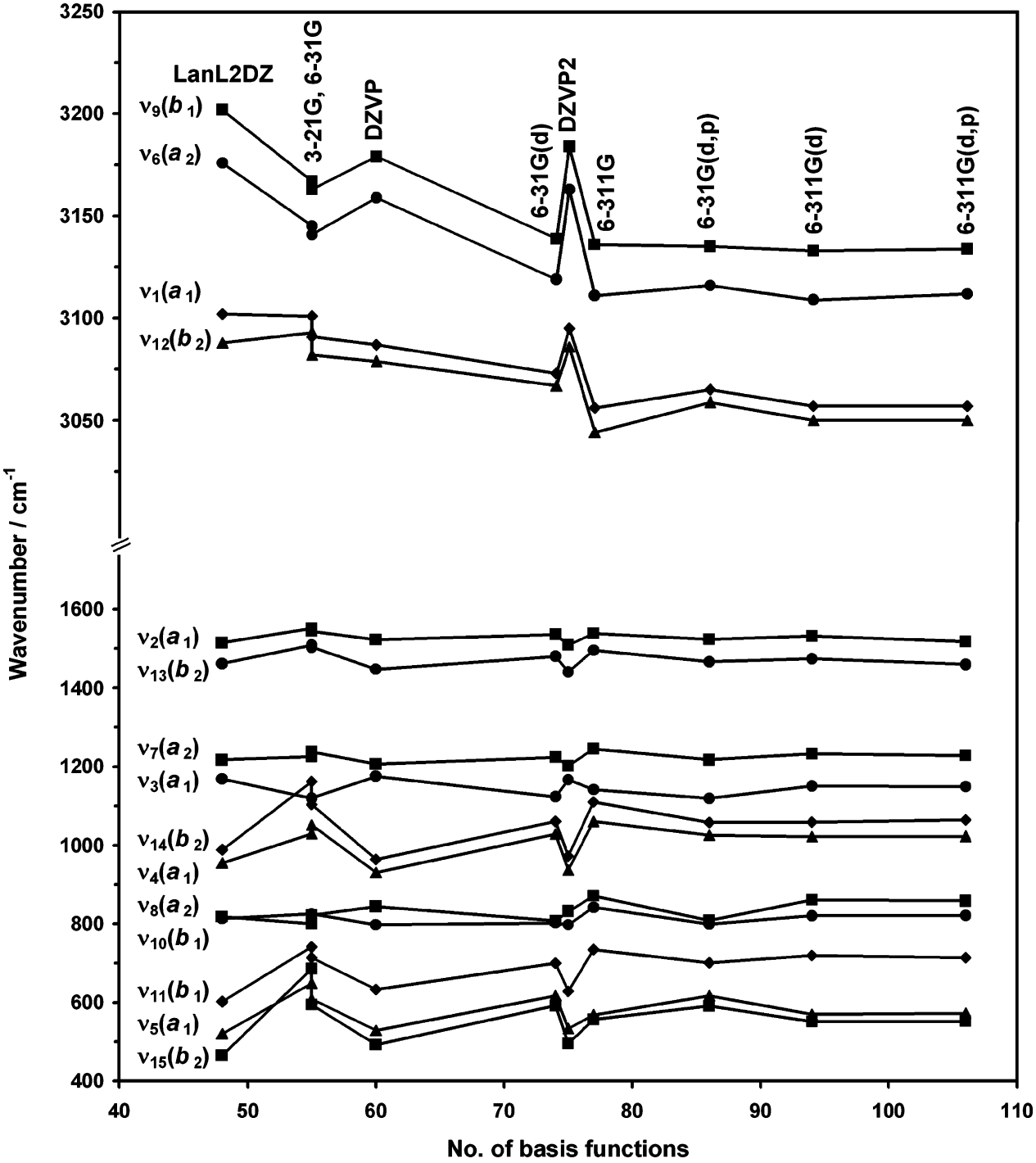

Figure 3. The effect of basis set on the B3-LYP vibrational spectrum of $[Ni(C_2H_4)]$.

note that the calculated vibrational spectrum agrees with the IR spectra of matrix isolated $[Ni(C_2H_4)]$ of Lee et al.,[51] i.e., the comparison of like-for-like, as opposed to the case for the geometric parameters, which compared the optimized geometry of $[Ni(C_2H_4)]$ with that of $[Ni(PPh_3)_2(C_2H_4)]$, for example.

Comparison of Different DFT and Hybrid DFT-SCF Methods. Having shown that the DZVP and LanL2DZ basis sets can provide accurate and reliable results in B3-LYP calculations, these two basis sets have been used to compare several DFT and hybrid DFT-SCF methods. The results of DFT calculations using different hybrid and pure DFT formalisms for $[Ni(C_2H_4)]$ are listed in Table 4 for the LanL2DZ basis set and Table 5 for the DZVP basis set. A significant variation in r(CC) (0.03 Å) was found for both basis sets. In all cases, calculations using LanL2DZ overestimate the carbon−carbon bond length while the DZVP basis set affords remarkably accurate bond lengths when used with hybrid functionals. With both basis sets, the BH and H method provides bond lengths that are shorter than all other methods. The pure DFT methods, B-LYP, PW91-LYP, and G96-LYP, all give longer CC bonds than any of the hybrid formalisms. In contrast to r(CC), r(NiC) is consistently underestimated when compared with experimental data; DZVP bond lengths are significantly shorter than the experimental values. At best, DZVP is within 0.08 Å of experimental values whereas LanL2DZ is within 0.06 Å. In contrast to the predicted bond lengths, the bond angles are largely insensitive toward the choice of formalism employed. Little variation is found for the θ(HCH) angle while θ(oop)

TABLE 4: Geometrical Parameters and Vibrational Spectra[a] of [Ni(C_2H_4)] Using the LanL2DZ Basis Set

		SVWN	PW91-LYP	G96-LYP	B-LYP	MPW-PW91	MPW1-PW91	B3-PW91	B3-P86	BH and H	BH and H-LYP	B1-LYP	B3-LYP	exp[b]
	r(CH)	1.102	1.100	1.100	1.100	1.100	1.091	1.093	1.092	1.088	1.084	1.091	1.093	
	r(CC)	1.443	1.460	1.462	1.462	1.456	1.445	1.447	1.445	1.434	1.444	1.450	1.450	1.431
	r(NiC)	1.873	1.931	1.927	1.934	1.918	1.905	1.908	1.904	1.875	1.906	1.919	1.918	1.991
	θ(NiCC)	67.4	67.8	67.7	67.8	67.7	67.7	67.7	67.7	67.5	67.7	67.8	67.8	69.8
	θ(CNiC)	45.3	44.4	44.6	44.4	44.6	44.6	44.6	44.6	45.0	44.5	44.4	44.4	42.1
	θ(oop)	13.7	13.6	14.2	13.9	14.0	14.5	14.6	14.3	14.8	15.3	14.4	14.3	
	θ(HCH)	114.7	114.9	114.6	114.7	114.6	114.3	114.3	114.4	114.1	114.0	14.4	114.4	
a_1	ν_1	3035	3022	3018	3017	3039	3135	3114	3119	3187	3202	3115	3102	2965.2
	ν_2	1458	1463	1472	1468	1474	1529	1519	1520	1553	1572	1523	1515	1468.2
	ν_3	1188	1139	1135	1135	1158	1192	1185	1189	1221	1194	1170	1169	1165.9
	ν_4	958	940	945	941	953	969	966	967	976	967	954	955	902.0
	ν_5	565	505	508	501	521	537	533	537	574	538	519	520	517.4
a_2	ν_6	3117	3101	3093	3092	3117	3212	3190	3195	3264	3273	3189	3176	
	ν_7	1166	1179	1182	1180	1183	1227	1219	1219	1249	1266	1225	1217	
	ν_8	799	792	789	790	800	830	824	825	843	838	821	819	
b_1	ν_9	3141	3127	3119	3119	3142	3237	3215	3220	3287	3299	3215	3202	3031.7
	ν_{10}	787	791	795	793	796	821	816	816	832	842	818	814	n.o.
	ν_{11}	579	576	587	580	587	613	608	607	631	635	606	602	601.8
b_2	ν_{12}	3024	3011	3007	3005	3027	3120	3099	3104	3169	3183	3100	3088	n.o.
	ν_{13}	1395	1416	1424	1421	1421	1471	1462	1462	1489	1516	1470	1462	1386.4
	ν_{14}	964	945	948	945	954	1003	993	993	1047	1043	995	988	907.0
	ν_{15}	490	448	451	446	465	484	478	480	504	480	465	465	502.2

[a] Bond lengths in Å, bond angles in degrees, and vibrational spectra in cm^{-1}. [b] Geometric parameters from ref 43, vibrational wavenumbers from ref 51.

TABLE 5: Geometrical Parameters and Vibrational Spectra[a] of [Ni(C_2H_4)] Using the DZVP Basis Set

		SVWN	PW91-LYP	G96-LYP	B-LYP	MPW-PW91	MPW1-PW91	B3-PW91	B3-P86	BH and H	BH and H-LYP	B1-LYP	B3-LYP	exp[b]
	r(CH)	1.103	1.100	1.099	1.100	1.100	1.091	1.093	1.092	1.089	1.084	1.091	1.093	
	r(CC)	1.428	1.444	1.443	1.445	1.439	1.431	1.432	1.430	1.423	1.432	1.434	1.434	1.431
	r(NiC)	1.848	1.908	1.906	1.912	1.890	1.871	1.876	1.873	1.840	1.872	1.892	1.892	1.991
	θ(NiCC)	67.3	67.8	67.8	67.8	67.6	67.5	67.6	67.5	67.2	67.5	67.7	67.7	69.8
	θ(CNiC)	45.5	44.5	44.5	44.4	44.8	45.0	44.9	44.9	45.5	45.0	44.5	44.5	42.1
	θ(oop)	13.6	13.5	13.7	13.6	13.8	14.7	14.5	14.4	15.5	15.7	14.3	14.2	
	θ(HCH)	114.4	114.6	114.4	114.5	114.4	113.9	114.0	114.1	113.6	113.5	114.1	114.2	
a_1	ν_1	3007	3008	3005	3004	3018	3111	3091	3095	3159	3181	3100	3087	2965.2
	ν_2	1462	1474	1481	1477	1478	1532	1523	1524	1555	1580	1533	1523	1468.2
	ν_3	1187	1146	1148	1144	1166	1192	1188	1190	1207	1187	1175	1175	1165.9
	ν_4	921	915	919	916	922	941	938	939	941	940	931	931	902.0
	ν_5	578	511	512	506	535	556	549	553	593	553	527	528	517.4
a_2	ν_6	3085	3082	3075	3075	3092	3185	3165	3169	3234	3250	3171	3159	
	ν_7	1148	1166	1171	1169	1168	1212	1204	1205	1234	1256	1215	1206	
	ν_8	825	819	824	820	825	846	844	846	846	849	846	844	
b_1	ν_9	3102	3102	3096	3096	3112	3205	3185	3189	3253	3270	3192	3179	3031.7
	ν_{10}	764	775	780	777	774	797	794	794	808	824	801	797	n.o.
	ν_{11}	607	609	614	611	617	642	637	636	655	662	636	632	601.8
b_2	ν_{12}	3001	3003	2999	2998	3012	3101	3082	3086	3148	3169	3091	3079	n.o.
	ν_{13}	1370	1405	1411	1408	1402	1450	1441	1441	1467	1502	1457	1447	1386.4
	ν_{14}	937	922	925	922	930	979	969	970	1017	1017	972	964	907.0
	ν_{15}	524	474	474	470	496	518	512	513	537	511	493	493	502.2

[a] Bond lengths in Å, bond angles in degrees, and vibrational spectra in cm^{-1}. [b] Geometric parameters from ref 43, vibrational wavenumbers from ref 51.

assumes one of three values depending on the *class* of formalism used. Pure DFT methods tend to give θ(oop) around 13.7°, hybrid functionals around 14.4°, and half-and-half functionals around 15.3°, regardless of basis set.

A detailed study of the effect of different DFT methods on systems such as [Ni(C_2H_4)] has not yet been reported. Bernardi et al. have compared the B3-LYP, B-LYP, and B-P86 methods using the DZVP basis set for [Ni(C_2H_4)$_2$] and found little variation between methods in the optimized geometries.[18] Furthermore, energy differences between isomers were found to be similar, indicating that the potential-energy surface is not sufficiently altered between methods. The differences in bond lengths between DFT methods reported by Bernardi et al. are similar to those in the present work, although for both basis sets, the SVWN and BH and H methods afford errant r(NiC) values. This is further evidenced by the small variations in vibrational wavenumbers displayed by the hybrid methods and the invariance of the mixing of ν(CC) and δ(CH_2) symmetry coordinates (vide infra). It has been noted previously[49] that hybrid DFT methods perform better than the pure DFT methods, and this is supported in the present work. Geometric parameters of the ethene moiety are better predicted using hybrid DFT methods and both DZVP and LanL2DZ basis sets. It is interesting to note that the pure DFT methods, with the exception of the SVWN method, better reproduce the nickel−carbon distances although the reason for this is unclear. From the data in Tables 4 and 5, it can be seen that DFT methods that employ Becke's three-parameter exchange functional, specifically B3-LYP and B3-PW91, give the best fit to experimental data.

The difference between the pure and hybrid DFT methods is best highlighted by the ν(CH) wavenumbers, which are consistently predicted to be significantly lower using the pure DFT

TABLE 6: Comparison of Calculated and Experimental Vibrational Spectra of [Ni(C_2H_4)]

mode		wavenumbers/cm^{-1} HF/LanL2DZ unscaled	MP2/LanL2DZ unscaled	B3-LYP/LanL2DZ unscaled	B3-LYP/LanL2DZ scaled	obs[a]	rel int obs[a]	rel int calc[b]	potential-energy distribution[b]
a_1	ν_1	3244	3142	3102	2952	2965.2	88	34	99 S_1
	ν_2	1626	1645	1515	1452	1468.2	4	1	75 S_2, 18 S_3
	ν_3	1132	1435	1169	1164	1165.9	89	41	77 S_3, 20 S_2
	ν_4	953	1063	955	880	902.0	100	3	97 S_4
	ν_5	579	424	520	525	517.4	7	7	97 S_5
a_2	ν_6	3296	3232	3176	3022			0	100 S_6
	ν_7	1321	1251	1217	1156			0	100 S_7
	ν_8	761	843	819	749			0	100 S_8
b_1	ν_9	3323	3256	3202	3046	3031.7	61	79	100 S_9
	ν_{10}	885	819	814	773	n.o.		2	100 S_{10}
	ν_{11}	711	314	602	549	601.8	25	53	100 S_{11}
b_2	ν_{12}	3220	3149	3088	2937	n.o.		66	100 S_{12}
	ν_{13}	1584	1513	1462	1391	1386.4	10	21	93 S_{13}
	ν_{14}	1122	845	988	919	907.0	0[c]	100	83 S_{14}, 10 S_{15}
	ν_{15}	525	513	465	472	502.2	15	17	90 S_{15}, 10 S_{14}

[a] From ref 51. [b] From the scaled B3-LYP/LanL2DZ calculations. [c] From the $\nu_4 + \nu_{14}$ combination band

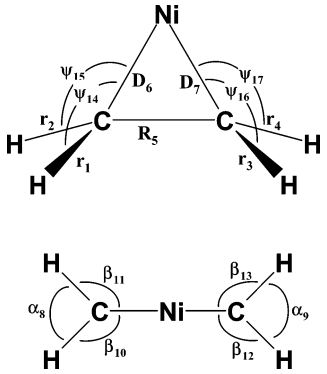

Figure 4. Definition of internal coordinates for [Ni(C_2H_4)].

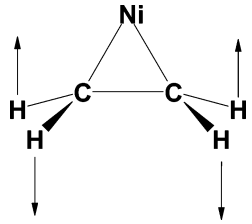

Figure 5. Definition of the ρ(ethene) coordinate.

TABLE 7: Symmetry Coordinates for Vibrations of [Ni(C_2H_4)]

species	description	coordinate
a_1	CH symm. stretch	$S_1 = r_1 + r_2 + r_3 + r_4$
a_1	CH_2 symm. deformation	$S_2 = \alpha_8 + \alpha_9 - \beta_{10} - \beta_{11} - \beta_{12} - \beta_{13}$
a_1	C=C stretch	$S_3 = R_5$
a_1	CH_2 symm. wag	$S_4 = \psi_{14} + \psi_{15} + \psi_{16} + \psi_{17}$
a_1	NiC symm. stretch	$S_5 = D_6 + D_7$
a_2	CH asymm. stretch	$S_6 = r_1 - r_2 - r_3 + r_4$
a_2	CH_2 asymm. rock	$S_7 = \beta_{10} - \beta_{11} - \beta_{12} + \beta_{13}$
a_2	CH_2 asymm. twist	$S_8 = \psi_{14} - \psi_{15} - \psi_{16} + \psi_{17}$
b_1	CH asymm. stretch	$S_9 = r_1 - r_2 + r_3 - r_4$
b_1	CH_2 asymm. rock	$S_{10} = \psi_{14} - \psi_{15} + \psi_{16} - \psi_{17}$
b_1	ethene rock	$S_{11} = \beta_{10} - \beta_{11} + \beta_{12} - \beta_{13}$
b_2	CH antisymm. stretch	$S_{12} = r_1 + r_2 - r_3 - r_4$
b_2	CH_2 antisymm. deformation	$S_{13} = \alpha_8 - \alpha_9 - \beta_{10} - \beta_{11} + \beta_{12} + \beta_{13}$
b_2	CH_2 antisymm. wag	$S_{14} = \psi_{14} + \psi_{15} - \psi_{16} - \psi_{17}$
b_2	NiC antisymm. stretch	$S_{15} = D_6 - D_7$

TABLE 8: Scaling Factors Used for [Ni(C_2H_4)]

internal coordinate	scale factor	internal coordinate	scale factor
r_1 to r_4	0.905	α_8 and α_9	0.910
R_5	0.980	β_{10} to β_{13}	0.900
D_6 and D_7	1.000	ψ_{14} to ψ_{17}	0.840

methods when compared to the hybrid functionals. The half-and-half methods both give slightly higher ν(CH) wavenumbers than the other hybrid methods. This behavior is mirrored to a lesser extent by the other vibrations. The pure DFT methods display a tendency to underestimate many of the vibrational modes when compared to the experimental spectra, i.e., the ν_3, ν_{11}, and ν(NiC) modes. This is an effect that would normally be exaggerated upon scaling. Analysis of the ν_3 vibration showed that all DFT methods predicted this mode to consist of an average of 77% ν(CC) coupled with $\delta(CH_2)$. The amount of mixing between these symmetry coordinates remained constant throughout the different hybrid methods. However, the pure B-LYP method predicted 88% ν(CC) coupled with a smaller contribution $\delta(CH_2)$. Of the hybrid functionals, those that incorporate Becke's three-parameter exchange functional, especially the B3-LYP method, tend to give the closest fit to the experimental data, without a significant degree of underestimation.

The vibrational wavenumbers obtained at the HF-SCF, post-SCF MP2, and hybrid DFT B3-LYP levels using the LanL2DZ basis set are compared in Table 6, which also includes the scaled quantum mechanical force field (SQM-FF) calculation wavenumbers and potential-energy distributions from the B3-LYP/LanL2DZ calculation. The internal coordinates used in the normal coordinate analysis follow those used by Lee et al.[51] and are shown in Figure 4, the symmetry coordinates and scale factors are given in Tables 7 and 8, respectively. The ethene rock vibration described in Table 7 corresponds to a tilting of the plane of the hydrogen atoms of the ethene molecule perpendicular to the carbon−nickel−carbon plane, depicted in Figure 5. Comparison of the unscaled spectra reveals the performance of B3-LYP to be significantly better than both the HF-SCF and MP2 methods. The inclusion of electron correlation by MP2 theory does not yield substantially more accurate vibrational spectra than HF-SCF. Indeed, for the LanL2DZ basis set, while the ν(CH) values are lower, a number of other modes are significantly less accurate at the MP2 level. All a_1 modes involving $\delta(CH_2)$ are overestimated by MP2, while the ν_{11} and ν_{14} modes are substantially underestimated. The improvement upon HF-SCF by B3-LYP is not surprising. However, the extent to which B3-LYP is superior to MP2 is unexpected. The totally symmetric vibrations, specifically the ν_3 mode, are significantly

TABLE 9: Geometric Parameters and Vibrational Spectra[a] of Transition Metal Ethene Complexes Calculated Using B3-LYP/LanL2DZ

		Fe(0)	Co(0)	Ni(0)	Cu(0)	Ru(0)	Rh(0)	Pd(0)	Ag(0)	Os(0)	Ir(0)	Pt(0)	Au(0)
	r(CH)	1.093	1.089	1.082	1.090	1.094	1.091	1.089	1.088	1.091	1.091	1.090	1.087
	r(CC)	1.455	1.402	1.484	1.497	1.467	1.440	1.416	1.351	1.468	1.465	1.459	1.367
	r(MC)	1.972	2.105	1.902	2.041	2.072	2.120	2.157	3.312	2.088	2.077	2.075	2.694
	θ(MCC)	68.4	70.6	67.0	68.5	69.3	70.2	70.8	78.2	69.4	69.4	69.4	75.3
	θ(CMC)	43.3	38.9	45.9	43.0	41.4	39.7	38.3	23.5	41.2	41.3	41.2	29.4
	θ(oop)	15.7	8.3	19.7	16.2	16.2	14.0	10.6	0.4	16.8	15.7	14.1	1.2
	θ(HCH)	112.8	115.9	112.0	114.8	114.6	114.0	115.7	116.6	112.9	113.5	114.8	116.9
a_1	ν_1	3097	3149	3244	3128	3073	3121	3143	3170	3109	3119	3130	3179
	ν_2	1520	1558	1626	1477	1482	1534	1548	1666	1518	1522	1520	1623
	ν_3	1135	1279	1132	1076	1140	1195	1251	1384	1145	1152	1169	1361
	ν_4	846	963	953	880	984	970	964	1011	1027	1033	1036	1018
	ν_5	489	293	579	409	476	413	365	46	474	495	480	94
a_2	ν_6	3167	3232	3296	3212	3144	3183	3223	3242	3182	3195	3213	3261
	ν_7	1214	1227	1321	1201	1207	1212	1227	1247	1205	1205	1209	1242
	ν_8	795	928	761	577	777	812	930	1055	817	824	850	1026
b_1	ν_9	3186	3258	3323	3241	3172	3217	3251	3278	3199	3213	3235	3293
	ν_{10}	796	827	885	821	824	821	830	844	821	812	819	843
	ν_{11}	635	497	711	548	659	636	563	127	763	762	739	330
b_2	ν_{12}	3081	3132	3220	3115	3056	3104	3126	3146	3089	3106	3117	3159
	ν_{13}	1472	1475	1584	1462	1459	1480	1473	1488	1487	1482	1473	1486
	ν_{14}	976	953	1122	864	1014	996	973	1008	1057	1054	1051	992
	ν_{15}	461	266	525	643	481	416	348	−32	547	519	488	−127

[a] Bond lengths in Å, bond angles in degrees, and vibrational spectra in cm^{-1}.

lower, and consequently more accurate, at the B3-LYP level than at MP2. Motions involving the nickel atom are best dealt with by B3-LYP; MP2 seems particularly poor at handling these modes; the ν_{11} ethene rock is some 300 cm^{-1} too low. This would indicate that MP2 theory has difficulty in modeling metal−olefin interactions. In this regard, it should be noted that it has, thus far, proved impossible to obtain an optimized geometry for [Ni(C_2H_4)] at the MP2/DZVP level.

The calculated relative IR intensities at the B3-LYP/LanL2DZ level are also listed in Table 6 along with the experimental data reported by Lee et al.[51] Despite the use of a relatively small basis set such as LanL2DZ, the agreement between calculated and experimental intensities is qualitatively reasonable. However, a large discrepancy is observed for the $\nu_4(a_1)$ $\omega(CH_2)_{sym}$ and the ν_{14} $\omega(CH_2)_{asym}$ modes. Here, ν_4 is predicted to be very weak, whereas the ν_{14} mode is predicted to be the strongest band in the infrared spectrum. This is clearly contrary to the assignments of Lee et al. The ν_{14} mode is consistently predicted to be the most intense band in the infrared spectrum at the B3-LYP level, while the ν_4 mode is always much weaker, although in the case of the B3-LYP/6-31G* calculation, the band assigned to ν_4 has 44% of the intensity of the ν_{14} band. However, according to Mitin et al.,[52] the 6-31G(d) basis set is flawed for late transition metals. By use of their modified 6-31G(d) basis set, the intensity of the ν_4 band is reduced to ca. 25%. It is therefore tentatively suggested that the assignments of the $\omega(CH_2)$ modes of the naturally abundant species of Lee et al. are reversed. Thus, the strongest band in the experimental IR spectrum at 902.0 cm^{-1} is assigned to ν_{14}. Reassignment of the strongest bands in the IR spectra of the [Ni($^{13}C_2H_4$)], [Ni(C_2D_4)], and [Ni($C_2H_2D_2$)] species is not inconsistent with the results of the B3-LYP/LanL2DZ or B3-LYP/DZVP calculations of the relevant isotopically substituted species, all of which predict the ν_{14} mode to be the strongest band in the IR spectrum while predicting ν_4 to be weak. Apart from the predicted strong intensity of the $\nu_{12}(b_2)$ $\nu(CH_2)_{asym}$ mode, which has not been observed experimentally, it is satisfying to note the agreement in the relative intensities at such a relatively modest level of theory.

In most cases, there is not much mixing of symmetry coordinates, although a notable degree of mixing between ν(CC) and $\delta(CH_2)$ coordinates is observed for the ν_2 and ν_3 modes, with the predominantly ν(CC) mode occurring at a lower wavenumber. A small degree of mixing is evident between the $\nu(NiC)_{asym}$ and $\omega(CH_2)_{asym}$ symmetry coordinates. The potential-energy distribution obtained at the scaled B3-LYP/LanL2DZ level is not significantly different from other methods. Little mixing between symmetry coordinates is observed apart from that between the ν(CC) and $\delta(CH_2)_{sym}$ coordinates, which has been suggested before based on both experimental data and empirical normal coordinate analysis but not quantified.[51,53−55] Furthermore, in many instances, the assignments of the ν(CC) and $\delta(CH_2)_{sym}$ modes have been wrongly reported[54,56,57] due to the mixing of these two modes leading to anomalous behavior upon isotopic substitution. Given that the behavior of these modes has proven to be a sensitive probe of the bonding of ethene−metal surfaces, i.e., di-σ, π, or metallocyclopropane, it would therefore seem fruitful to investigate the behavior and mixing of the ν(CC) and $\delta(CH_2)_{sym}$ modes on a wide variety of surfaces through SQM-NCA. It should be noted that the predicted degree of mixing increases considerably at the MP2 level. The ν(CC), $\delta(CH_2)_{sym}$, and $\omega(CH_2)_{sym}$ symmetry coordinates are heavily mixed in the ν_2, ν_3, and ν_4 modes as are the $\omega(CH_2)_{asym}$ and $\nu(NiC)_{asym}$ symmetry coordinates in the ν_{14} and ν_{15} modes.

Trends within the Transition Metals. Having determined that B3-LYP/LanL2DZ and B3-LYP/DZVP are the most efficient and accurate methods for the determination of the structure and spectral features of [Ni(C_2H_4)], the applicability of these methods were then tested on other ethene complexes with transition metals. The effect of variation of metal on the geometries and vibrational spectra of zerovalent ethene complexes is shown in Table 9 for B3-LYP/LanL2DZ and in Table 10 for B3-LYP/DZVP. The omission of the third-row elements in Table 10 is a consequence of the limited range of metals for which the DZVP basis set has been defined. The general trend is that on going from left to right across a row, the carbon−carbon bond distance decreases, although this trend is not evident for the first row transition metals. The shortening of r(CC) may be expected to be accompanied by a lengthening of the metal−carbon bond and a decrease in θ(oop) values. The decrease in θ(oop) is observed for both second and third row

TABLE 10: Geometric Parameters and Vibrational Spectra[a] of Transition Metal Ethene Complexes Calculated at the B3-LYP/DZVP Level

		Fe(0)	Co(0)	Ni(0)	Cu(0)	Ru(0)	Rh(0)	Pd(0)	Ag(0)
	r(CH)	1.093	1.090	1.093	1.090	1.094	1.091	1.089	1.088
	r(CC)	1.435	1.403	1.434	1.490	1.440	1.417	1.388	1.339
	r(MC)	1.955	2.000	1.892	1.997	2.080	2.133	2.213	3.598
	θ(MCC)	68.5	69.5	67.7	68.1	69.7	70.6	71.7	79.3
	θ(CMC)	43.0	41.0	44.5	43.8	40.5	38.8	36.6	21.4
	θ(oop)	15.8	10.7	14.2	17.5	15.6	13.4	9.1	0.2
	θ(HCH)	112.5	115.1	114.2	114.0	114.6	114.5	116.0	116.7
a_1	ν_1	3083	3119	3087	3110	3064	3109	3141	3164
	ν_2	1533	1554	1523	1481	1502	1541	1580	1688
	ν_3	1149	1233	1175	1075	1167	1208	1276	1373
	ν_4	872	908	931	866	955	935	928	968
	ν_5	505	324	528	414	459	388	317	33
	ν_6	3150	3195	3159	3189	3131	3176	3217	3233
a_2	ν_7	1211	1217	1206	1197	1208	1213	1222	1235
	ν_8	823	921	844	562	767	853	974	1056
	ν_9	3164	3214	3179	3212	3155	3201	3240	3260
b_1	ν_{10}	789	809	797	813	820	816	822	831
	ν_{11}	649	592	632	556	631	605	522	94
	ν_{12}	3073	3109	3079	3104	3051	3097	3129	3148
b_2	ν_{13}	1462	1459	1447	1456	1452	1464	1463	1472
	ν_{14}	961	941	964	854	965	947	924	948
	ν_{15}	491	397	493	629	470	401	314	25

[a] Bond lengths in Å, bond angles in degrees, and vibrational spectra in cm^{-1}.

metals but again, not for the first row. The increase in r(MC) is only seen for the second row metals. Upon descending a group, r(CC) increases markedly between the first and second rows for groups 8 and 9 followed by a smaller increase between the second and third rows. With the exception of [Co(C_2H_4)], using the LanL2DZ basis set, r(MC) and θ(oop) both increase upon descending the iron and cobalt groups. No discernible trends are observed in the nickel or copper groups, although the calculations indicate that both gold(0) and silver(0) ethene complexes have substantially longer metal−carbon bonds and shorter carbon−carbon bonds.

With the exception of [Co(C_2H_4)], using the DZVP basis set, the ν(CH) vibrations increase when crossing a row from left to right. The calculated ν(CH) vibrations of [Fe(C_2H_4)] are significantly higher than those observed for [Fe(C_2H_4)] in an argon matrix,[58] for which the IR spectra have been interpreted in terms of Fe interacting with one or two hydrogen atoms. This interpretation was supported by the observation that ν(C═C) was very close to that of free C_2H_4. Experimentally, the ν(CC) modes have been found to have the following trend: [Co(C_2H_4)] > [Ni(C_2H_4)] > [Cu(C_2H_4)],[59,51,60] and this effect is well reproduced in Tables 9 and 10. The predominantly ν(CC) mode occurs at 1224 cm^{-1} for [Co(C_2H_4)], 1166 cm^{-1} for [Ni(C_2H_4)], and 1156 cm^{-1} for "[$Cu_2(C_2H_4)_2$]", cf. 1233, 1175, and 1075 cm^{-1}, respectively, in Table 10. Similar trends are observed for the CH_2 deformations which have been observed[51] at 1504 cm^{-1} for [Co(C_2H_4)], 1468 cm^{-1} (or 1490 cm^{-1} according to Ozin[59]) for [Ni(C_2H_4)], and ca. 1474 cm^{-1} for [Cu(C_2H_4)]. These trends are well reproduced with the DZVP basis set but somewhat less satisfactorily with the LanL2DZ basis set. For both $\nu(MC)_{sym}$ and $\nu(MC)_{asym}$, a general decrease in wavenumber can be seen on going from the left of a row, although in this case, comparison with experimental data is difficult. Imaginary wavenumbers are predicted for $\nu(MC)_{asym}$ for [Au(C_2H_4)] and [Ag(C_2H_4)] of 127i cm^{-1} and 32i cm^{-1}, respectively. Notwithstanding the copper group metals, which show the opposite effect, the ν(CH) wavenumbers decrease upon descending a group.

It is difficult to compare trends in the calculated values with experimental data due to the lack of self-consistent, systematic experimental studies. As the calculations are for zerovalent single binary metal−ethene complexes, comparison with a real structure may be impossible. For example, [Ag(C_2H_4)] intuitively seems unlikely to exist and difficulties have been encountered in attempting to detect such binary complexes by vibrational spectroscopies, especially Raman.[60] This is reflected in the optimized geometry using both LanL2DZ and DZVP basis sets, which yield large r(AgC) and small θ(oop). It is known that ethene does not adsorb onto clean silver surfaces. Ethene adsorption onto silver has been modeled by Avdeev and Zhidomirov by an $Ag_{12}O_3$ cluster.[61] Adsorption was proposed to occur at surface defect sites, represented by a cationic vacancy and also due to partial oxidation of the surface.

It is relatively facile to compare the trends on descending group 10 although no examples of palladium(0)−ethene complexes are known. It is interesting that the extent of distortion of the ethene moiety follows the order Ni > Pt > Pd rather that Ni > Pd > Pt. This effect has also been observed by Nunzi et al.[16] who investigated the bonding of [$M(PH_3)_2(C_2X_2)$] complexes using DFT methods, where M = Ni, Pd, Pt and X = H, F, CN. Nunzi et al. demonstrated that for these complexes, π back bonding is more significant than σ bonding. Furthermore, the extent of π back bonding for [Pd(C_2H_4)] was found to be half that of [Pt(C_2H_4)]. The anomalous distortion of ethene was also noted by Ziegler and co-workers[17] who incorporated quasi-relativistic effects into their DFT models. It is suggested that the increased distortion and shorter r(MC) for [Pt(C_2H_4)] than [Pd(C_2H_4)] was due to the increased importance of relativistic effects for platinum compared to palladium. It may not be strictly necessary to include quasi-relativistic effects when modeling structures and vibrational spectra of transition metal complexes as B3-LYP/LanL2DZ calculations can produce satisfactory results at considerably less computational cost.

In terms of vibrational spectra, comparison of the IR and Raman spectra of Zeise's salt, $[PtCl_3(C_2H_4)]^+$, with its palladium analogue reveal that the trends are comparable with those predicted by the data in Table 9. A band in the Raman spectrum of $[PdCl_3(C_2H_4)]^+$, assigned by Bencze et al.[62] to ν(CC), at 1526 cm^{-1} corresponds to our calculated value for ν_2, at 1548 cm^{-1}. Hiraishi[63] reported a band in the Raman spectrum of Zeise's salt at 1522 cm^{-1}, which we calculate at 1520 cm^{-1}. Similarly, the band assigned to $\delta(CH_2)_{sym}$ by Bencze et al. in the spectrum

of the palladium salt at 1267 cm^{-1}, predicted to occur at 1251 cm^{-1}, corresponds to a band at 1241 cm^{-1} in the spectrum of Zeise's salt, predicted at 1169 cm^{-1}. Despite the fact that the experimental data is for M^{2+} complexes and the calculated spectra are for M^0 complexes, the *trends* upon changing the coordinated metal remain faithfully reproduced. Indeed, the calculated ν(CC) mode compares poorly to the Pt^{2+}, Zeise's salt. However, comparison with Pt^0 complexes, such as [Pt-$(PPh_3)_2(C_2H_4)$], shows a much more satisfactory fit. Crayston and Davidson[64] observed ν(CC) at 1120 cm^{-1} (cf. 1169 cm^{-1} in Table 9). Furthermore, the assignment of the 1120 and 1570 cm^{-1} bands to ν(CC) and $\delta(CH_2)_{sym}$, respectively, were supported by normal coordinate analysis.[65]

The most important indicators of surface adsorption are the ν(CC) and $\delta(CH_2)_{sym}$ modes. As these modes are both totally symmetric, they are stronger in the Raman spectrum than in the IR spectrum. However, in Raman studies of ethene adsorbed on platinum group metals, these bands can be comparatively weak. This problem has been overcome by deposition of an overlayer of platinum group metal over a roughened SERS-active gold substrate, a technique pioneered by Weaver and co-workers.[66−68] This leads to an enhanced Raman scattering mechanism from the underlying gold substrate, but the spectrum is characteristic of the platinum group overlayer. Thus, SERS spectra for ethene adsorbed on Rh, Pd, Ir, and Pt have been reported.[66] Experimentally, the ν(CC) and $\delta(CH_2)_{sym}$ vibrations follow the order Rh < Pd < Ag and Ir < Pt < Au. These trends are well reproduced in the data in Tables 9 and 10. The $\delta(CH_2)_{sym}$ mode is calculated 2 cm^{-1} higher in [Ir(C_2H_4)] than [Pt(C_2H_4)], but this is not inconsistent with experiment as the $\delta(CH_2)_{sym}$ mode was found to occur at the same energy for ethene adsorbed on both Ir and Pt. Taking into account the fact that the SERS spectra were recorded in an electrochemical environment, the calculated spectra give a satisfactory agreement, although the band wavenumbers are a little high; i.e., ethene adsorbed on Pd displays SERS bands at 1514 and 1244 cm^{-1}, whereas our calculations yield values of 1548 and 1251 cm^{-1}.

Conclusions

To elucidate the most efficient method for performing ab initio calculations on the geometric structure and vibrational spectra of transition-metal−alkene complexes, and possibly adsorbed species on metal surfaces, [Ni(C_2H_4)] has been used as a model. The geometric structure has been optimized using a number of different basis sets and levels of theory. The vibrational spectrum has also been simulated from these optimized geometries. Comparison of these optimized geometries and vibrational spectra with experimental data reveals that the all-electron DZVP and DZVP2 basis sets afford the closest fit to experimental data. The ECP LanL2DZ basis set has been shown to give results that are of almost comparable quality to the DZVP and DZVP2 basis sets but at a fraction of the computational cost. By use of both the DZVP and LanL2DZ basis sets, different levels of theory and different density functional formalisms were tested to find the optimum level of theory to be used for modeling transition metal complexes. It has been demonstrated that DFT methods are best suited to dealing with transition-metal complexes. Furthermore, hybrid DFT methods, specifically those that use Becke's three-parameter exchange functional, provide a better fit to the experimental data than the "pure" DFT methods. The B3-LYP method has proved to be by far the most desirable method of calculation. B3-LYP is not only a more efficient method of calculation than the expensive MP2 method, but it also yields vibrational wavenumbers, which are *systematically* higher than experimental values as opposed to MP2 calculations. The MP2 level of theory displays a more varied effect when comparing calculated results with experimental values. Thus, B3-LYP is more amenable to the application of a physically meaningful set of scaling factors that MP2.

From the results of B3-LYP calculations, especially in conjunction with the LanL2DZ basis set, the potential-energy distributions of the vibrations of [Ni(C_2H_4)] were investigated. The traditional assignments of the ν_2 and ν_3 modes to the ν(CC) and $\delta(CH_2)_{sym}$ modes, respectively, which have been used as indications into the nature of bonding between metal and olefinic hydrocarbons, were found to be incorrect. B3-LYP consistently gave the ν_3 mode around 1100 cm^{-1} to be predominantly CC stretching coupled with some CH_2 deformation, whereas the ν_2 mode around 1500 cm^{-1} was found to be mainly $\delta(CH_2)_{sym}$ coupled to some extent with ν(CC). This is opposite to the assignments that have often been given in the past. In a recent case,[53] the CC stretch was given at 1242 cm^{-1} and the CH_2 deformation at 1512 cm^{-1} but these were considered to be an almost 50:50 mix of both vibrations. The results of the potential-energy distributions show that the ratio is roughly 75:25. A reassignment of the $\omega(CH_2)_{sym}$ and $\omega(CH_2)_{asym}$ modes is also suggested by the calculated potential-energy distributions and IR intensities.

The suitability of different basis sets and levels of theory have also been tested for $[Ni(C_2H_4)]^{2+}$. Although it was possible to obtain optimized geometries in C_{2v} symmetry, imaginary wavenumbers, corresponding to $\nu(NiC)_{asym}$, indicate that these geometries corresponded to transition states or saddle points on the potential-energy surface. Eigenvector following revealed true energy minima corresponding to C_s, or in some cases C_1, symmetry, where the nickel atom was bound only to one carbon atom.

The results of the ab initio calculations on different metal-(0)−ethene complexes reveal that the simple model used can reproduce the trends shown in most cases on going from metal to metal; i.e., the behavior of the ν(CC) and $\delta(CH_2)_{sym}$ bands upon descending the Group 10 metals follows that observed experimentally. The simple model used here provides a moderately inexpensive yet highly useful, qualitatively accurate simulation of the structure and vibrational spectra of ethene complexes with transition metals, although it should be noted that the lack of self-consistent experimental data precludes a definitive evaluation of the performance of the model. Further, it is noted that the model is limited, partly by computational resources, to use with simple transition-metal complexes; modeling of metal surfaces *must* incorporate many more metal atoms, in the form of clusters or slabs, to truly define the site and mode of adsorption. In the case of adsorption energies, it is imperative that surface reconstruction is included whenever possible. In the case of electrochemical studies, modeling of the variation of electric field should also provide interesting results.

Acknowledgment. We thank the University of Dundee for a University Scholarship (to B.D.A.).

References and Notes

(1) Herges, R.; Papafilippopoulos, A. *Angew. Chem., Int. Ed. Engl.* **2001**, *40*, 4671.

(2) Schore, J. E. *Chem. Rev.* **1988**, *88*, 1081.

(3) Reppe, W.; Schweckendieck, W. J. *Liebigs Ann. Chem.* **1948**, *104*, 560.

(4) Hyla-Kryspin, I.; Koch, J.; Gleiter, R.; Klettke, T.; Walther, D. *Organometallics* **1998**, *17*, 4724.
(5) Wilke, G. *Angew. Chem.* **1988**, *100*, 189.
(6) Wilke, G. *Angew. Chem., Int. Ed. Engl.* **1988**, *27*, 185.
(7) Rosch, N.; Hoffmann, R. *Inorg. Chem.* **1974**, *13*, 11.
(8) Upton, T. H.; Goddard, W. A. *J. Am. Chem. Soc.* **1978**, *100*, 321.
(9) Akermark, B.; Almemark, M.; Almlof, J.; Backvall, J. E.; Roos, B.; Stoegard, A. *J. Am. Chem. Soc.* **1977**, *99*, 4617.
(10) Basch, H.; Newton, M. D.; Moskowitz, J. W. *J. Chem. Phys.* **1978**, *69*, 584.
(11) Itoh, H.; Kunz, A. B. *Chem. Phys. Lett.* **1979**, *66*, 531.
(12) Pitzer, R. M.; Schaefer, H. F. *J. Am. Chem. Soc.* **1979**, *101*, 7176.
(13) Widmark, P. O.; Roos, B. O.; Siegbahn, P. E. M. *J. Phys. Chem.* **1985**, *89*, 2180.
(14) Zhang, D.-J.; Liu, C.-B.; Liu, Y.-J.; Hu, H. Q. *Chin. J. Chem.* **2002**, *20*, 220.
(15) Pierloot, K.; Persson, B. J.; Roos, B. O. *J. Phys. Chem.* **1995**, *99*, 3465.
(16) Nunzi, F.; Sgamellotti, A.; Re, N.; Floriani, C. *J. Chem. Soc., Dalton Trans.* **1999**, 3487.
(17) Li, J.; Schreckenbach, G.; Ziegler, T. *Inorg. Chem.* **1995**, *34*, 3245.
(18) Bernardi, F.; Bottoni, A.; Calcinari, M.; Rossi, I.; Robb, M. A. *J. Phys. Chem. A* **1997**, *101*, 6310.
(19) Chatt, J.; Duncanson, L. A. *J. Chem. Soc.* **1953**, 2939.
(20) Dewar, M. J. S. *Bull. Soc. Chim. Fr.* **1951**, C71.
(21) Frisch, M. J.; Trucks, G. W.; Schlegel, H. B.; Scuseria, G. E.; Robb, M. A.; Cheeseman, J. R.; Zakrzewski, V. G.; Montgomery, J. A., Jr.; Stratmann, R. E.; Burant, J. C.; Dapprich, S.; Millam, J. M.; Daniels, A. D.; Kudin, K. N.; Strain, M. C.; Farkas, O.; Tomasi, J.; Barone, V.; Cossi, M.; Cammi, R.; Mennucci, B.; Pomelli, C.; Adamo, C.; Clifford, S.; Ochterski, J.; Petersson, G. A.; Ayala, P. Y.; Cui, Q.; Morokuma, K.; Malick, D. K.; Rabuck, A. D.; Raghavachari, K.; Foresman, J. B.; Cioslowski, J.; Ortiz, J. V.; Stefanov, B. B.; Liu, G.; Liashenko, A.; Piskorz, P.; Komaromi, I.; Gomperts, R.; Martin, R. L.; Fox, D. J.; Keith, T.; Al-Laham, M. A.; Peng, C. Y.; Nanayakkara, A.; Gonzalez, C.; Challacombe, M.; Gill, P. M. W.; Johnson, B. G.; Chen, W.; Wong, M. W.; Andres, J. L.; Head-Gordon, M.; Replogle, E. S.; Pople, J. A. *Gaussian 98*, revision A.5; Gaussian, Inc.: Pittsburgh, PA, 1998.
(22) Hay, P. J.; Wadt, W. R. *J. Chem. Phys.* **1985**, *82*, 270.
(23) Hay, P. J.; Wadt, W. R. *J. Chem. Phys.* **1985**, *82*, 299.
(24) Wadt, W. R.; Hay, P. J. *J. Chem. Phys.* **1985**, *82*, 284.
(25) Godbout, N.; Salahub, D. R.; Andzelm, J.; Wimmer, E. *Can. J. Chem.* **1992**, *70*, 560.
(26) Andzelm, J.; Wimmer, E. *J. Chem. Phys.* **1992**, *96*, 1280.
(27) Hariharan, P. C.; Pople, J. A. *Chem. Phys. Lett.* **1972**, *66*, 217.
(28) Dunning, T. H., Jr.; Hay, P. J. *Modern Theoretical Chemistry*; Schaefer, H. F., III, Ed.; Plenum: New York, 1976; Vol. 3, p 1.
(29) Adamo, C.; Barone, V. *J. Comput. Chem.* **1998**, *19*, 419.
(30) Gill, P. M. W. *Mol. Phys.* **1996**, *89*, 433.
(31) Adamo, C.; Barone, V. *Chem. Phys. Lett.* **1997**, *274*, 242.
(32) Lee, C.; Yang, W.; Parr, R. G. *Phys. Rev. B* **1988**, *37*, 785.
(33) Perdew, J. P.; Chevary, J. A.; Vosko, S. H.; Jackson, K. A.; Pederson, M. R.; Singh, D. J.; Fiolhais, C. *Phys. Rev. B* **1993**, *48*, 4978.
(34) Perdew, J. P.; Burke, K.; Wang, Y. *Phys. Rev. B* **1996**, *54*, 16533.
(35) Perdew, J. P.; Chevary, J. A.; Vosko, S. H.; Jackson, K. A.; Pederson, M. R.; Singh, D. J.; Fiolhais, C. *Phys. Rev. B* **1992**, *46*, 6671.
(36) Becke, A. D. *J. Chem. Phys.* **1993**, *98*, 5648.
(37) Becke, A. D. *J. Chem. Phys.* **1996**, *104*, 1040.
(38) Perdew, J. P. *Phys. Rev. B* **1986**, *33*, 8822.
(39) Becke, A. D. *J. Chem. Phys.* **1993**, *98*, 1372.
(40) Schachtschneider, J. A. *Vibrational Analysis of Polyatomic Molecules*; Technical Report Nos. 231 and 57; Shell Development Co.: Houston TX., 1964 and 1965; Parts V and VI.
(41) Pulay, P.; Fogarasi, G.; Pongor, G.; Boggs, J. E.; Vargha, A. *J. Am. Chem. Soc.* **1983**, *105*, 7037.
(42) Schroeder, W.; Poerschke, K. R.; Tsay, Y. H.; Krueger, C. *Angew. Chem.* **1987**, *99*, 953.
(43) Cheng, P. T.; Cook, C. D.; Koo, C. H.; Nyburg, S. C.; Shiomi, M. T. *Acta Crystallogr. Sect. B* **1971**, *27*, 1904.
(44) Carr, R. G.; Sham, T. K.; Eberhardt, W. E. *Chem. Phys. Lett.* **1985**, *113*, 63.
(45) Demuth, J. E. *Surf. Sci.* **1979**, *84*, 315.
(46) Bernardi, F.; Bottoni, A.; Rossi, I. *J. Am. Chem. Soc.* **1998**, *120*, 7770.
(47) Alexander, B. D.; Dines, T. J., unpublished results.
(48) Bernardo, C. P. G. M.; Gomes, J. A. N. F. *THEOCHEM* **2001**, *542*, 263.
(49) Huang, H. Y.; Padin, J.; Yang, R. T. *J. Phys. Chem. B* **1999**, *103*, 3206.
(50) Bogel, H.; Tobisch, S.; Nowak, T. *Int. J. Quantum Chem.* **1998**, *69*, 387.
(51) Lee, Y. K.; Hannachi, Y.; Xu, C.; Andrews, L.; Manceron, L. *J. Phys. Chem.* **1996**, *100*, 11228.
(52) Mitin, A. V.; Baker, J.; Pulay, P. *J. Chem. Phys.* **2003**, *118*, 7775.
(53) Merle-Mejean, T.; Cosse-Mertens, C.; Bouchareb, S.; Galan, F.; Mascetti, J.; Tranquille, M. *J. Phys. Chem.* **1992**, *96*, 9148.
(54) Papai, I.; Mink, J.; Fournier, R.; Salahub, D. R. *J. Phys. Chem.* **1993**, *97*, 9986.
(55) Cooper, E.; Raval, R. *Surf. Sci.* **1995**, *331*−*333*, 94.
(56) Ozin, G. A.; Power, W. J.; Upton, T. H.; Goddard, W. A. *J. Am. Chem. Soc.* **1978**, *100*, 4750.
(57) Huber, H.; Ozin, G. A.; Power, W. J. *J. Am. Chem. Soc.* **1976**, *98*, 6508.
(58) Kafafi, Z. H.; Hauge, R. H.; Margrave, J. L. *J. Am. Chem. Soc.* **1985**, *107*, 7550.
(59) Hanlan, A. J. L.; Ozin, G. A.; Power, W. J. *Inorg. Chem.* **1978**, *17*, 3648.
(60) Merle-Méjean, T.; Bouchareb, S.; Tranquille, M. *J. Phys. Chem.* **1989**, *93*, 1197.
(61) Avdeev, V. I.; Zhidomirov, G. M. *Surf. Sci.* **2001**, *492*, 137.
(62) Bencze, E.; Papai, I.; Mink, J.; Goggin, P. L. *J. Organomet. Chem.* **1999**, *584*, 118.
(63) Hiraishi, J. *Spectrochim. Acta, Part A*, **1969**, *25*, 749.
(64) Crayston, J. A.; Davidson, G. *Spectrochim. Acta, Part A* **1986**, *42*, 1385.
(65) Crayston, J. A.; Davidson, G. *Spectrochim. Acta, Part A* **1987**, *43*, 559.
(66) Mrozek, M. F.; Weaver, M. J. *J. Phys. Chem. B* **2001**, *105*, 8931.
(67) Mrozek, M. F.; Xie, Y.; Weaver, M. J. *Anal. Chem.* **2001**, *73*, 5953.
(68) Weaver, M. J.; Zou, S.; Chan, H. Y. H. *Anal. Chem.* **2000**, *72*, 38A.